

Article

Optimization of Destressing Parameters of Water Jet Slits in Rock Burst Coal Seams for Deep Mining

Yingyuan Wen ^{1,2}, Anye Cao ^{1,*}, Chuanhong Ding ³, Yang Hu ^{1,4}, Chengchun Xue ¹ , Yujie Peng ¹ and Shikang Song ⁵

¹ School of Mines, China University of Mining and Technology, Xuzhou 221116, China; wenyinyuan2010@126.com (Y.W.); hy19816253577@163.com (Y.H.); xccxue@126.com (C.X.); TB22020022A41@cumt.edu.cn (Y.P.)

² School of Geology and Mining Engineering, Xinjiang University, Urumqi 830046, China

³ Datun Energy Company Limited, Xuzhou 221600, China; chuanhong2018@yahoo.com

⁴ Yunnan Coal Mine Safety Technology Center Co., Ltd., Kunming 650000, China

⁵ Shaanxi Zhengtong Coal Ind Co., Ltd., Xianyang 713600, China; jiangshuihaiyue@126.com

* Correspondence: caoanye@163.com

Abstract: Mining in deep coal seams is characterized by high ground stress, often accompanied by coal and rock dynamic disasters such as rock bursts. High-pressure water jet slotting technology can relieve pressure and reduce the stress concentration on the coal seam, which is one of the effective pressure relief measures in rock burst coal seams for deep mining. Reasonable pressure relief parameters are an important influence on the effectiveness of pressure relief achieved by a high-pressure water jet. This paper uses theoretical analysis and numerical simulation to analyze the principle of high-pressure water jet pressure relief and rock burst prevention, and a theoretical calculation model of six key pressure relief parameters is constructed. The optimal values of each pressure relief parameter are obtained, and good pressure relief effect is achieved in a certain rock burst risk area. The research results showed that (1) parameters such as drilling spacing–slit radius, drilling depth–slit length, and slotting cutting spacing–slotting cutting width have a great influence on the pressure relief effect, and there is a significant interaction between the parameters, while the strength of the coal seam also has a significant effect on the selection of the parameters and the pressure relief effect. (2) The displacement, vertical stress, plastic zone, elastic energy, impact risk index, and the cost of pressure relief can be used to comprehensively evaluate the quality and economy of the pressure relief effect, and the optimal pressure relief parameters of high-pressure water jet slotting under specific physical force properties of the coal seam can be obtained. (3) High-pressure water jet technology with optimal pressure relief parameters was applied to No. 3 connecting the roadway in the 730 mining area of a mine studied, and field monitoring showed that indicators such as microseismic frequency, total energy, and spatial concentration significantly decreased. Moreover, the accuracy of the theoretical model of high-pressure water jet slotting pressure relief parameter optimization is reliable in the relevant technical parameters of coal seam slotting. It is believed that the model can be used to design the high-pressure water jet slotting pressure relief parameters in deep rock burst coal seams.

Keywords: rock burst; deep mining; water jet slotting; parameter optimization; numerical simulation



Citation: Wen, Y.; Cao, A.; Ding, C.; Hu, Y.; Xue, C.; Peng, Y.; Song, S. Optimization of Destressing Parameters of Water Jet Slits in Rock Burst Coal Seams for Deep Mining. *Processes* **2023**, *11*, 1056. <https://doi.org/10.3390/pr11041056>

Academic Editors: Junwen Zhang, Xuejie Deng and Zhaohui Wang

Received: 7 March 2023

Revised: 26 March 2023

Accepted: 29 March 2023

Published: 31 March 2023



Copyright: © 2023 by the authors. Licensee MDPI, Basel, Switzerland. This article is an open access article distributed under the terms and conditions of the Creative Commons Attribution (CC BY) license (<https://creativecommons.org/licenses/by/4.0/>).

1. Introduction

Rock bursts generally pose a serious threat to either normal underground mining activities or surface buildings, and even cause serious injury to miners [1,2]. Currently, mining conditions have exhibited a dramatic deterioration with increased mining depth [3–5] and a large number of coal burst accidents occurring in China. It was on 20 October 2018 that a coal burst occurred in Longyun Coal Mine, in which the 174 m length long dip entry collapsed, associated with 21 workers being killed [6]. The other coal

burst occurred on 9 June 2019 and was reported in the Longjiapu coal mine, resulting in the 220 m length roadway being damaged and injures to miners [7]. It was on 22 February 2020 that the coal burst occurred in the Xinjulong coal mine which also resulted in a huge loss [8]. That is, coal bursts have been one of the most serious dynamic disasters in deep coal mines.

The high-pressure water jet (HPWJ) technique has showed its effectiveness in preventing rock bursts in the deep mining coal seam [9–11]. Based on the high-pressure water as the power to impact the coal seam, the uniform annular groove in the track around a particular plastic failure zone as well as the weakening area will then be generated [12–14]. Many scholars have studied the coal-breaking mechanism of the HPWJ. Cao et al. [15] analyzed the failure mode of rock treated by the HPWJ. Xue et al. [16] revealed the coal-breaking mechanism of the HPWJ and the effectiveness of pressure relief based on pressure relief and permeability increase technology. Zhang [17] analyzed the mechanical mechanism of coal breaking via the HPWJ, which is divided into two stages: the stress wave effect and secondary crack propagation effect. Lu et al. [18] studied the pulse mechanism of the HPWJ and revealed three dynamic characteristics. The above research showed that the HPWJ slotting technique forms an ample pressure relief space by forming slotting grooves associated with a good application for high stress release in the inner coal seam.

How to determine the scientific and reasonable parameters of the HPWJ is particularly important for ensuring the overall stability of the roadway and minimizing the risk of rock bursts. There are three factors affecting the pressure relief effect of the HPWJ [19–22], which are nozzle structure parameters, coal seam mechanical properties, and pressure relief design parameters. The pressure relief effect of the HPWJ slotting technique with different parameters has been experimentally and numerically investigated. The numerical simulation conducted by Gu et al. [23] studied the influence law of various influencing factors on the crack formation of HPWJ via the numerical simulation method. Li [24] also carried out the numerical simulation, whereby the result of which showed that the HPWJ slotting pressure relief and permeability enhancement technology were effective in the prevention and controlling of dynamic disasters. Gao et al. [25] established the THM model to explore the sensitivity of the borehole slit to various influencing factors. Zhang et al. [26] repeated the process of the HPWJ pressure relief via numerical analysis, whereby the main parameters accounted for in which covered the coal seam permeability and washing length. The fact, however, is that the HPWJ slotting process is complicated. Most importantly, the unreasonable selection of slotting parameters will easily cause multiple disturbances of the surrounding rock of the roadway.

Although current research has investigated HPWJ technology from various aspects and made solid contributions, there has been no systematic research on the reasonable design of pressure relief parameters for a water jet based on actual site requirements. Correspondingly, there is a lack of quantitative analysis and reasonable determination methods for the key pressure relief design parameters of water jets on site. Against this background, the present research is devoted to establishing an optimization theoretical model accounting for six parameters (e.g., drilling spacing–slotting radius, drilling depth–slotting length, and slotting cutting spacing–slotting cutting width), in which the theoretical value of parameters are calculated based on the physical and mechanical properties of the coal seam. Based on the analysis of displacement, stress, energy, and impact risk index obtained using numerical simulation, combined with the economic cost of the site, the optimal pressure relief parameters are obtained, which can effectively guide the field coal seam pressure relief work.

2. Pressure Relief Principle and Parameter Optimization Model of the HPWJ Slotting

2.1. Effect of the HPWJ Slotting on Coal Seam Stress Reduction and Energy Release

According to the strength weakening and blanking reduction theory, reducing the accumulated energy in coal and rock mass is an effective method to eliminate the occurrence of rock bursts [27]. When the coal and rock mass are under the triple stress status, there is

lots of elastic energy in the HPWJ cutting after unloading. It is around the borehole that the stress value is greater than that of the concentration of coal strength and the plastic deformation occurs. Note that the coal within the plastic failure zone is still in the form of the inelastic state. Based on the elasticity theory [28], if the stress and strain of coal and rock show a linear relationship, the elastic strain energy density per unit volume can be expressed by the following equation:

$$U_s = \frac{\sigma_{s1}^2 + \sigma_{s2}^2 + \sigma_{s3}^2 - 2\mu_s \cdot \sigma_{s1} \cdot \sigma_{s2} - 2\mu_s \cdot \sigma_{s2} \cdot \sigma_{s3} - 2\mu_s \cdot \sigma_{s1} \cdot \sigma_{s3}}{2E_s} \quad (1)$$

where σ_{s1} , σ_{s2} , and σ_{s3} are the maximum, intermediate, and minimum principal stresses of the basic element under the dominance of the stress field, respectively, μ_s is the value of Poisson's ratio of the coal seam, and E_s represents the elastic modulus of the coal seam in the plastic failure zone.

The fish language was adopted to edit the elastic strain energy density of the basic element in the process of pressure relief of the HPWJ slit as per Formula (1). The distribution of elastic energy density of the roadway side before and after the HPWJ can be seen in Figure 1.

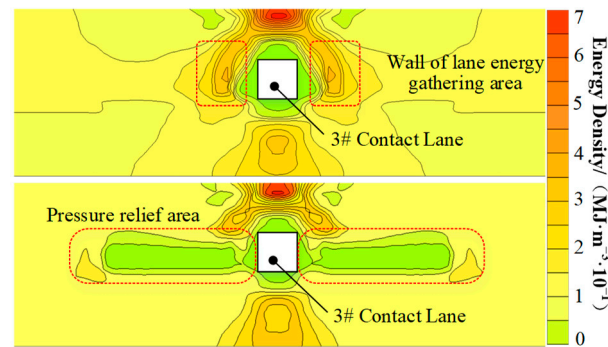


Figure 1. Diagram of energy variation before and after pressure relief.

It is apparent in Figure 1 that the accumulated energy on both sides of the roadway is significantly reduced after the pressure relief, with an average reduction value of 0.28 MJ and an average reduction rate of 70.2%. Due to the lack of seam relief, there is an energy-gathering area in the roadway roof featured with a “circular” distribution. The area 5 m upon the roadway roof is an energy-gathering peak area, with a peak value of 0.65 MJ. Compared with the unrelieved zone, the internal energy release of the coal bodies on both sides of the roadway is evident after the HPWJ cutting and pressure relief. It significantly reduces the energy concentration and eliminates the occurrence of rock bursts around the roadway.

To explore the HPWJ cutting before and after unloading stress evolution, the stress distribution of the high-pressure water jet under a certain parameter was analyzed via numerical simulation. The critical parameter of the HPWJ cutting after unloading stress distribution and the pressure relief parameters of borehole spacing S , drilling depth H , protection coal pillar L , cutting hole spacing D , and cutting hole radius R were selected for reference. The variation rule of vertical stress before and after pressure relief is shown in Figure 2.

As seen in Figure 2, the limit stress value of the dynamic manifestation of the rock burst that occurred in the coal seams on both sides of the roadway is defined as σ_m . If the value of peak stress (σ_a) accumulated in a coal seam is higher than σ_m , the coal seam will be destroyed instantly and a rock burst correspondingly occurs. Note that the vertical stress curve shown in Figure 2 is in the form of the “single-peak type” and the peak stress peak is about two times that of the original rock stress (σ_n) before pressure relief. The vertical stress curve of the roadway wall after pressure relief is bimodal and two stress peaks in the roadway coal wall can be expressed as σ_b and σ_c , respectively, where $\sigma_a > \sigma_b > \sigma_c > \sigma_n$.

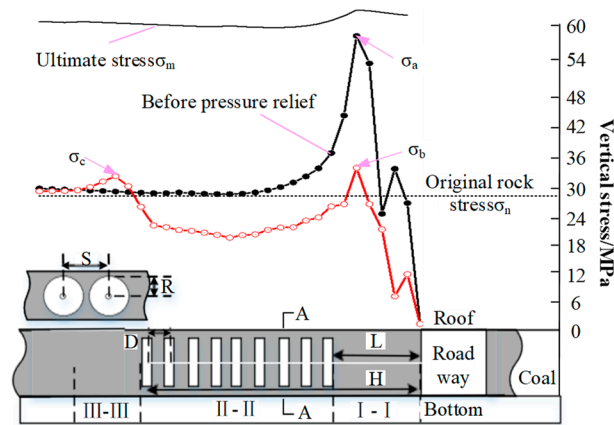


Figure 2. Diagram of stress variation before and after pressure relief.

As per Figure 2, the stress distribution can be divided into three regions:

- (1) Zone I-I is the protective coal pillar cutting area with the length of L . Within this zone, the peak stress σ_b is about 1.20 times that of the original rock stress, 5 m from the coal wall. Because of the existence of a roadway support body, the slot pressure relief is adopted to ensure the support system stability. The length (L) of the uncut section should be less than the distance between the coal wall of the roadway and the peak stress within the coal seam.
- (2) Zone II-II is the pressure relief zone of the slit, with an average stress reduction rate of 30.8%. The average stress concentration coefficient of the roadway surroundings is less than 1, which is the central pressure relief zone of the slit with the HPWJ. The stress-relaxation area associated with the loosened coal seam produces a large failure area. Therefore, high energy cannot be accumulated and permanent yield deformation can be formed in the coal seam in this area. Meanwhile, it is helpful for reducing the stress concentration in the high-pressure jet drilling area.
- (3) Area III-III is affected by the HPWJ cutting. The stress peak σ_c is about 1.12 times the original rock stress. It was distributed in the area about 3 m away from the bottom of the pressure relief hole. Attributed to the cutting groove, the stress increases in some areas and then is restored to the original rock stress.

2.2. Optimization Model of Borehole Spacing and Slit Radius Parameters

The grooves attributed to the HPWJ slotting can be divided into the crushing zone [11], plastic zone, and elastic zone from the inside to the outside. As shown in Figure 3, the tracks of the adjacent boreholes are divided into three types.

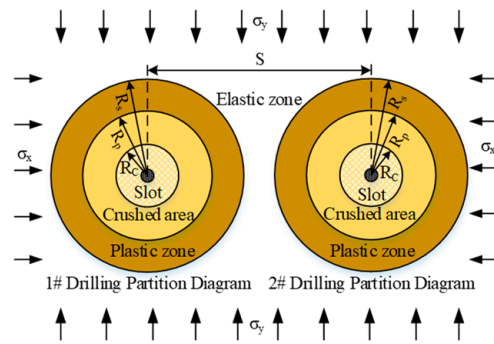


Figure 3. Schematic diagram of the theoretical model of the parameters of drill hole spacing and slot radius.

According to the principle of unchanged coal volume before and after slot collapse, the relationship between the slot broken zone radius R_p , final broken zone radius R_{p1} , and slot radius R_C can be obtained as follows [28]:

$$P^* \pi (R_p^2 - R_C^2) = \pi R_{p1}^2 \quad (2)$$

where P is the swelling fragmentation coefficient of the collapsed coal seam, $P = 1.2 \sim 1.5$.

For ease of reference, it is assumed that the slot collapse area will not increase with a rise in coal fissure, namely, $R_p = R_{p1}$. As a result, the value can be expressed as below:

$$R_p = \sqrt{\frac{P}{P-1}} R_C \quad (3)$$

If the coal failure in the seam area follows the straight-line Coulomb criterion, there will be a mass of random cracks. In this case, the actual plastic zone radius will be more significant and the real radius of the plastic zone R_S will be as follows [29]:

$$R_S = \left\{ \frac{[\sigma_y(1 + \lambda) + 2c \cot \varphi](1 - \sin \varphi)}{2c \cot \varphi} \right\}^{\frac{1 - \sin \theta}{2 \sin \theta}} * \left\{ 1 + \frac{\sigma_y(1 - \lambda)(1 - \sin \theta \cos 2\theta)}{[\sigma_y(1 + \lambda) + 2c \cot \varphi] \sin \varphi} \right\} n R_p \quad (4)$$

where R_S is the plastic zone radius of the slot, m; σ_y is the horizontal stress of the coal rib zone, MPa; λ is the lateral pressure coefficient; c is the coal cohesion, MPa; φ is the internal friction angle of the coal rib zone, °; θ is the circumferential angle, °; and n is the correction coefficient, $n = 1.1 \sim 1.3$.

The effect of the pressure relief will be much more obvious when the spacing of drilling holes is less than or equal to two times the plastic zone radius R_S of the slot. If so, the cutting coverage area will thus be generated. To avoid this situation, the spacing of drilling holes should meet the following relationship:

$$2R_C \leq S \leq 2R_S \quad (5)$$

2.3. Optimization Model of Drilling Depth–Slit Length Parameters

We assume that the investigated subject in the present research is isotropic and homogeneous and that the HPWJ cutting and pressure releasing are carried out in rectangular roadways driven within the coal rib zone (m and n are the width and height of the roadway, respectively) when the roadway is in the in-plane strain state, and the stress model of which can be seen in Figure 4.

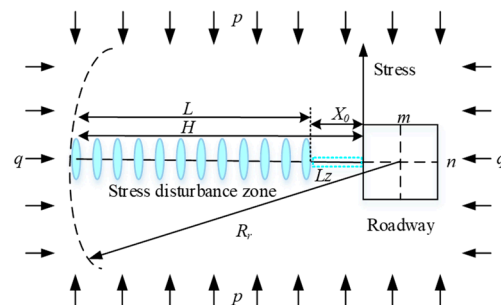


Figure 4. Schematic diagram of the theoretical model of drilling depth–slot length parameter.

Associated with the redistribution of the stress, the stress disturbance zone will be then formed around the roadway. The drilling depth of the HPWJ cutting should cover the disturbance zone R_r . Considering the effect of stress concentrations, the range of the stress disturbance zone should be more extensive than that of the calculated value upon the

original rock stress. Taking the coefficient as 1.2, the content of roadway stress disturbance can be expressed as seen in the following formula [30]:

$$\begin{cases} R_r = \sqrt{\frac{1}{5\%}} a \omega = 5.364a \\ a = \frac{m+n}{\pi} \end{cases} \quad (6)$$

where R_r is the radius of the stress disturbance zone; a is the equivalent radius of the rectangular tunnel; and m and n are the width and height of the rectangular roadway, respectively. ω is the correction coefficient calculated in the stress disturbance area, $\omega = 1.2$.

Because the HPWJ slotting starts from the bottom of the hole, the slotting length should cover the ultimate strength area of the coal rib zone at the side of the roadway. The distance between the rib to the ultimate strength area of the coal rib zone can be calculated by the following equation [31]:

$$X_0 = \ln \left[\frac{\lambda(\sigma_{y\max} \cos \alpha \tan \phi + 2c - M\gamma_0 \sin \alpha)}{\lambda(2c - M\gamma_0 \sin \alpha) + 2P_x \tan \phi} \right] * \frac{M\lambda}{2 \tan \phi} \quad (7)$$

where M is the thickness of the mined coal rib zone, m; λ is the lateral pressure coefficient; α is the coal rib zone dip angle, °; ϕ is the friction angle at the interface between the coal seam and the roof and the floor, °; c is the cohesion of the coal seam, MPa; P_x is the binding force of the roadway support on the coal wall along the radial direction, MPa; and γ^0 is the average volume force of the coal, MPa.

The ultimate strength of the roadway wall coal can be calculated by the following formula [31]:

$$\sigma_{y\max} = \delta \eta \sigma_c = 2.729(\eta \sigma_c)^{0.729} \quad (8)$$

in which η is the rheological coefficient of coal and rock, and σ_c is the UCS of coal and the rock test block, MPa.

On the basis of the above discussion, the pressure relief effect will be obvious if the length of the slit segment (L) is greater than or equal to $H - X_0$. With the consideration of the stability of the roadway support, no seam cutting is carried out in the area L_Z of the roadway support body. Therefore, the drilling depth and the length of the slit segment of the HPWJ cutting can be expressed as follows:

$$\begin{cases} L \geq 5.364a \\ H - X_0 \leq L \leq H - L_Z \end{cases} \quad (9)$$

2.4. Groove Cutting Spacing–Groove Cutting Width Parameter Optimization Theoretical Model

In general, the redistributed stress around the slot is made of the elastic zone, plastic zone, and crushing zone with the application of the HPWJ on the slot. The theoretical model of the slot cutting spacing–slot cutting width of the HPWJ slot cutting technique is shown in Figure 5.

According to the above analysis of the radius of the crushing zone and plastic zone, the width of the crushing zone and plastic zone can be obtained as follows:

$$\begin{cases} R_{PK} = \sqrt{\frac{P}{P-1}} R_C - R_C \\ R_{Sk} = R_P \left\{ \frac{[\sigma_y(1+\lambda) + 2c \cot \phi](1 - \sin \varphi)}{2c \cot \varphi} \right\}^{\frac{1 - \sin \theta}{2 \sin \theta}} * \left\{ 1 + \frac{\sigma_y(1-\lambda)(1 - \sin \theta \cos 2\theta)}{[\sigma_y(1+\lambda) + 2c \cot \phi] \sin \varphi} \right\} n - R_P \end{cases} \quad (10)$$

where R_{Pk} is the width of the slot crushing zone, m; R_{Sk} is the width of the plastic zone of the slot, m.

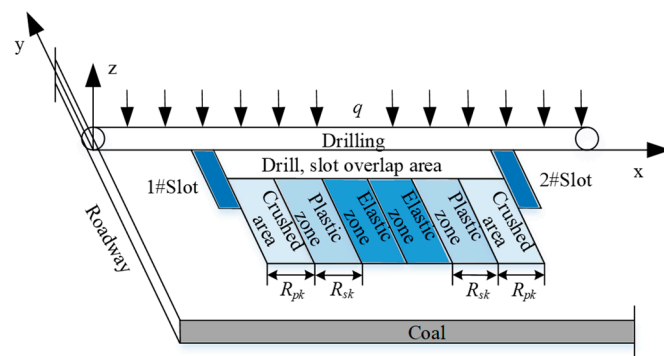


Figure 5. Schematic diagram of the theoretical model of slot cutting distance–slot cutting width parameter.

Similarly, the pressure relief effect will be better when the groove cutting distance is less than or equal to two times $(R_{sk} + R_{pk} + l/2)$.

Herein, the groove cutting distance can be expressed as follows:

$$D \leq 2\left(R_{pk} + R_{sk} + \frac{l}{2}\right) \leq 2R_P \left(\left\{ \frac{[\sigma_y(1+\lambda)+2c \cot \varphi](1-\sin \varphi)}{2c \cot \varphi} \right\}^{\frac{1-\sin \theta}{2 \sin \theta}} * \left\{ 1 + \frac{\sigma_y(1-\lambda)(1-\sin \theta \cos 2\theta)}{[\sigma_y(1+\lambda)+2c \cot \varphi] \sin \varphi} \right\} n - 1 \right) + 2R_C \left(\sqrt{\frac{p}{p-1}} - 1 \right) + l \quad (11)$$

2.5. Theoretical Calculation Value of Pressure Relief Parameters of Slit of the HPWJ

Taking the 730 mining area of the coal mining in the engineering case in Section 4 as an example, the coal cohesion $c = 1.0$ MPa, the internal friction angle $\varphi = 32^\circ$, the coal seam dip angle $\alpha = 8^\circ$, the coal compressive strength $\sigma_c = 21.10$ MPa, the rheological coefficient $\eta = 0.5$, the side pressure coefficient $\lambda = 0.47$, the circular angle $\theta = 45^\circ$, the breaking–swelling coefficient $P = 1.35$, and the correction coefficient $n = 1.2$. The length of the roadway side bolt is 2.4 m. The binding force on the coal wall along the radial direction of the roadway $P_x = 0.25$ MPa, and the average volume force $\gamma^0 = 0.014$ MPa.

In view of the maximum slit radius of the HPWJ (2.0 m), the coal parameters are substituted into the theoretical optimization model and the theoretical calculation values of each pressure relief parameter are, respectively, as follows:

- (1) When the slit radius $R_C = 0.5$ m, 1.0 m, 1.5 m, and 2.0 m, the theoretical calculation value S of the hole spacing is 1.0–3.0 m, 2.0–7.0 m, 3.0–10.0 m, and 4.0–14.0 m;
- (2) The theoretical calculation value of the drilling depth $H \geq 14.16$ m, and the theoretical calculation value of the slit length L is $H-5.58 \leq L \leq H-2.4$;
- (3) According to the field test results and previous research results, when the slot cutting width $L = 0.1$ –0.3 m and the slot radius $R_C = 0.5$ m, 1.0 m, 1.5 m, and 2.0 m, the theoretical calculation values of the slot cutting spacing D are $D \leq 3.82$, $D \leq 7.36$, $D \leq 10.9$, and $D \leq 14.34$.

3. Numerical Simulation Analysis of Slit Parameters of the HPWJ

3.1. Numerical Model Construction

This numerical simulation was conducted on the basis of the geological conditions of the concentrated roadways in the 730 mining area of coal mining in the engineering case with the averaged buried depth of 1080 m. To reflect the real roadway-supporting unloading process after unloading, the displacement, stress, and the evolution characteristics of the parameters (e.g., energy), the FLAC^{3D} was adopted with the consideration of the anchor cable and anchor support. Moreover, a 15 m protective coal pillar was set at both ends of No.3 contact lanes. According to the lithological characteristics of the geological borehole map and laboratory test results, the schematic diagram of the FLAC^{3D} model is shown in

Figure 6. Both the physical and mechanical properties of the surrounding rocks are listed in Table 1.

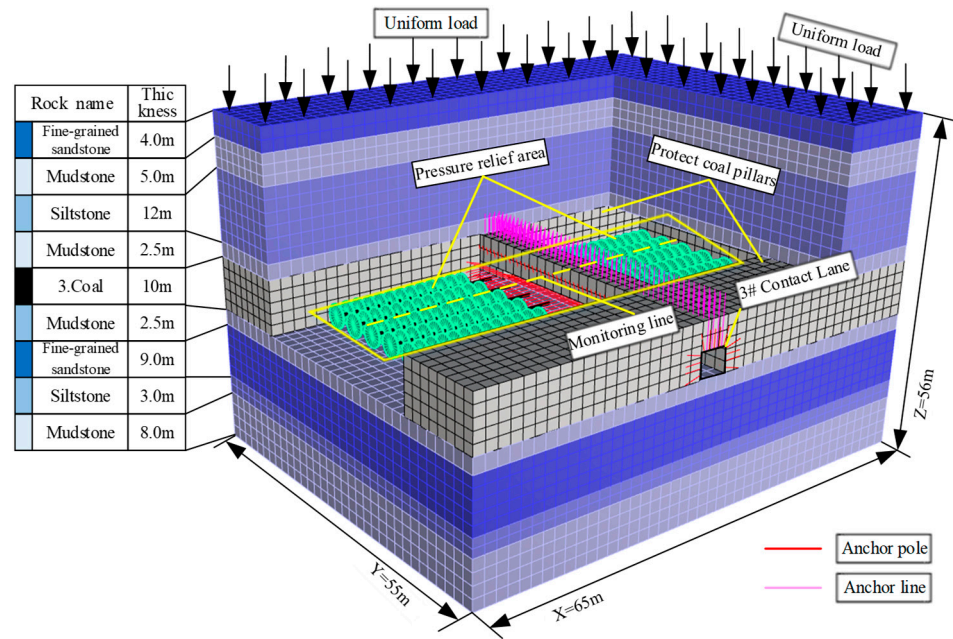


Figure 6. Schematic diagram of FLAC3D model and pressure relief area.

Table 1. Physical and mechanical parameters of coal strata.

The Name of the Coal and Rock	The Bulk Modulus/GPa	The Shear Modulus/GPa	The Density/Kg.m ⁻³	The Angle of Internal Friction	The Cohesion/MPa
No.3 coal	2.41	0.98	1400	32	1.0
Mudstone	3.55	1.82	2380	38	2.2
Siltstone	5.22	3.38	2446	38	8.0
Fine grained sandstone	6.44	3.35	2600	36	8.5

3.2. Numerical Simulation Scheme

As an extension of the theoretical analysis results presented in Section 2, the six factors of borehole spacing, slit radius, drilling depth, slit length, slot cutting spacing, and slot cutting width were investigated for their effect on pressure relief in the roadway.

The simulation scheme for drilling spacing and slit radius parameters is shown in Table 2.

Table 2. Numerical simulation scheme for drilling spacing–slit radius.

The Project	The Slot Radius/m	The Borehole Spacing/m	The Project	The Slot Radius/m	The Borehole Spacing/m	The Project	The Slot Radius/m	The Borehole Spacing/m
1	0.5	1.0	11	1.5	4.0	21	2.0	7.0
2	0.5	2.0	12	1.5	5.0	22	2.0	8.0
3	0.5	3.0	13	1.5	6.0	23	2.0	9.0
4	1.0	2.0	14	1.5	7.0	24	2.0	10.0
5	1.0	3.0	15	1.5	8.0	25	2.0	11.0
6	1.0	4.0	16	1.5	9.0	26	2.0	12.0
7	1.0	5.0	17	1.5	10.0	27	2.0	13.0
8	1.0	6.0	18	2.0	4.0	28	2.0	14.0
9	1.0	7.0	19	2.0	5.0			
10	1.5	3.0	20	2.0	6.0			

The simulation scheme for drilling depth–slit length parameters is shown in Table 3.

Table 3. Numerical simulation scheme for drilling depth–slit length.

The Project	Drill Hole Depth/m	Length of the Slot/m	The Project	Drill Hole Depth/m	Length of the Slot/m	The Project	Drill Hole Depth/m	Length of the Slot/m
1	15	10.0	6	19	16.0	11	25	20.0
2	15	12.0	7	21	16.0	12	25	22.0
3	17	12.0	8	21	18.0	13	27	22.0
4	17	14.0	9	23	18.0	14	27	24.0
5	19	14.0	10	23	20.0			

The simulation scheme for groove cutting spacing–groove cutting width parameters can be seen in Table 4.

Table 4. Numerical simulation scheme for groove cutting spacing–groove cutting width.

The Project	Spacing/m	Width/m	The Project	Spacing/m	Width/m	The Project	Spacing/m	Width/m
1	0.1	1.0	6	0.3	2.0	11	0.2	4.0
2	0.2	1.0	7	0.1	3.0	12	0.3	4.0
3	0.3	1.0	8	0.2	3.0	13	0.1	5.0
4	0.1	2.0	9	0.3	3.0	14	0.2	5.0
5	0.2	2.0	10	0.1	4.0	15	0.3	5.0

In this paper, the displacement, vertical stress, plastic zone, elastic energy, impact risk index, and pressure relief cost after pressure relief were used as indicators to evaluate the effectiveness of the HPWJ pressure relief.

According to the minimum energy principle [32], the energy consumed is always the energy of the uniaxial stress state under the action of triaxial stress, namely

$$U_{\min} = \frac{\sigma_c^2}{2E} \quad (12)$$

where E is the elastic modulus, MPa.

The ratio of the elastic energy after pressure relief to the minimum energy required for dynamic failure is defined as the impact risk index K , the value of which can be obtained via the following equation:

$$K = \frac{U_S}{U_{\min}} \quad (13)$$

3.3. Pressure Relief Effect Analysis

3.3.1. Analysis of Drilling Spacing and Slit Radius Parameters

Take the constant value of the slit radius to be 2.0 m and the spacing between holes to be 4.0 m, 5.0 m, and 6.0 m. In this case, the displacement field, stress field, plastic zone, and elastic energy density of the roadway side after pressure relief seem to be different.

(1) Changing the rule of the displacement field

The variation rule of the displacement field is shown in Figure 7a, for which the existence of the support body of the roadway is considered and the wall displacement is small. For example, when the spacing between boreholes is 4.4 m, the maximum value is 4.31 mm.

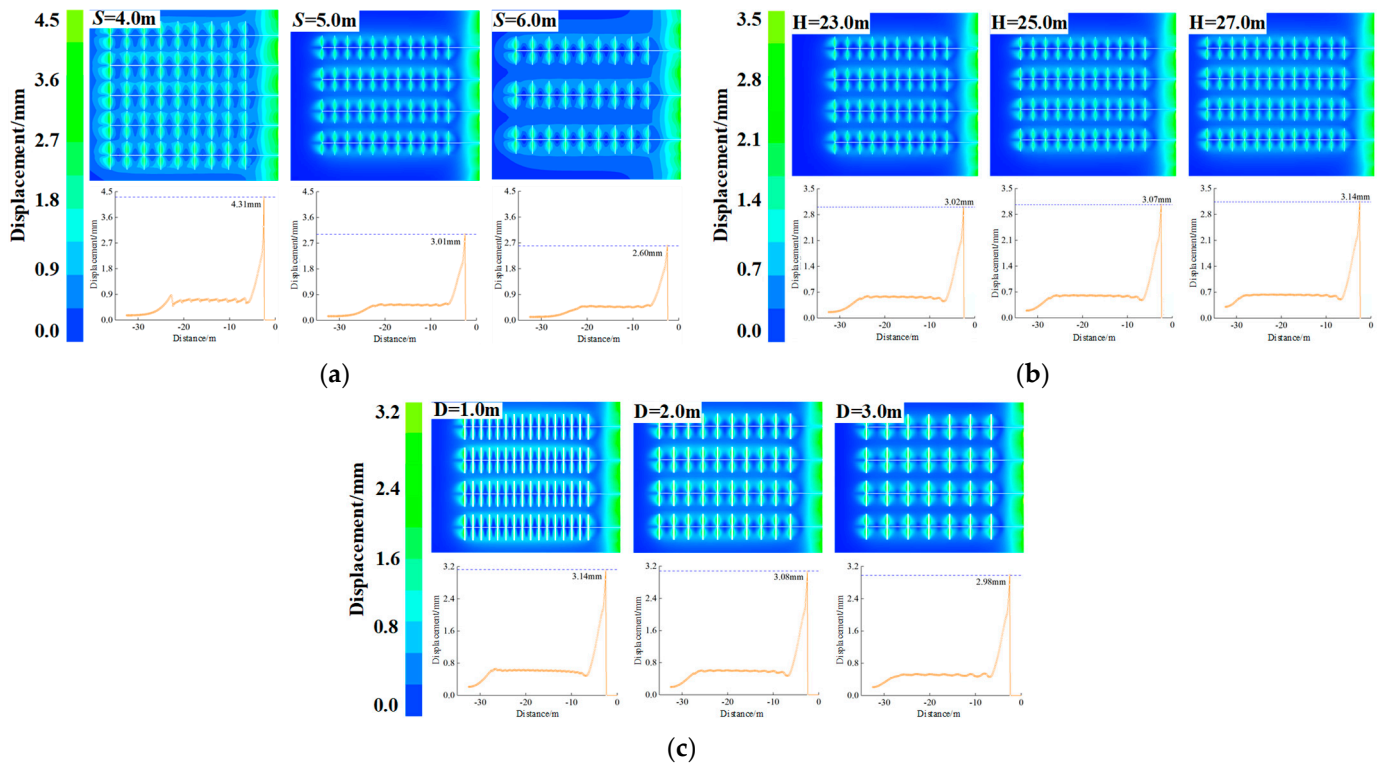


Figure 7. Displacement field change law diagram under different parameters: drilling spacing and slit radius (a), drilling depth and slit length (b), and slot cutting spacing and slot cutting width (c).

(2) Variation law of stress field

The effective pressure-releasing area of the roadway wall coal rib zone, for which the vertical stress is reduced to below 27 MPa (original rock stress), is shown in Figure 8. It is apparent that the effective pressure-releasing area of the HPWJ cutting area at some stages (II, III, and IV) is more extensive. Correspondingly, the range significantly decreases with the increased spacing between boreholes.

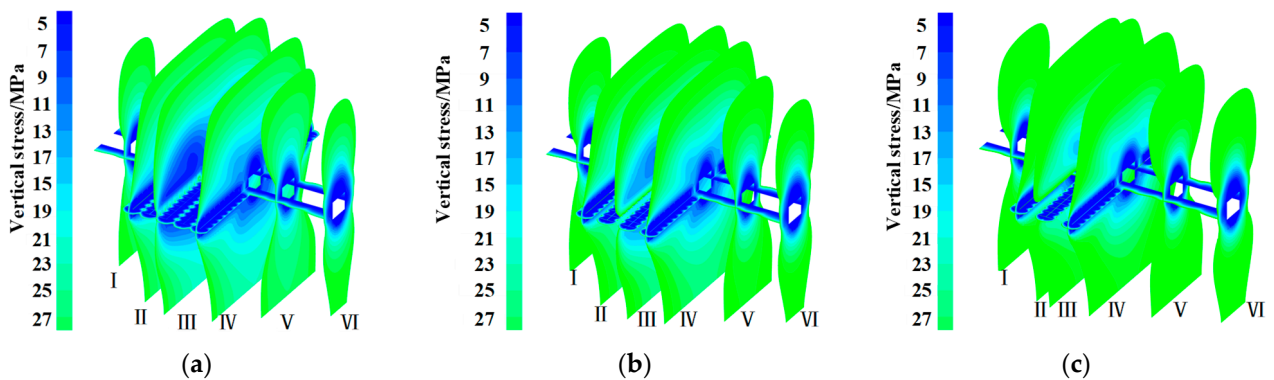


Figure 8. The effective pressure-releasing area of the coal rib zone in the roadway with the borehole spacing of 4.0 m (a), 5.0 m (b), and 6.0 m (c). I–VI represent the cross section along the strike, with a spacing of 10 m.

As per Figure 9, the average vertical stress in the relief area is 9 MPa, 13 MPa, and 16.8 MPa, when the spacing between holes is 4.0 m, 5.0 m, and 6.0 m, associated with the stress concentration coefficients of 0.33, 0.48, and 0.62, respectively. Note that the relief effect gradually decreases with the increased spacing between different boreholes.

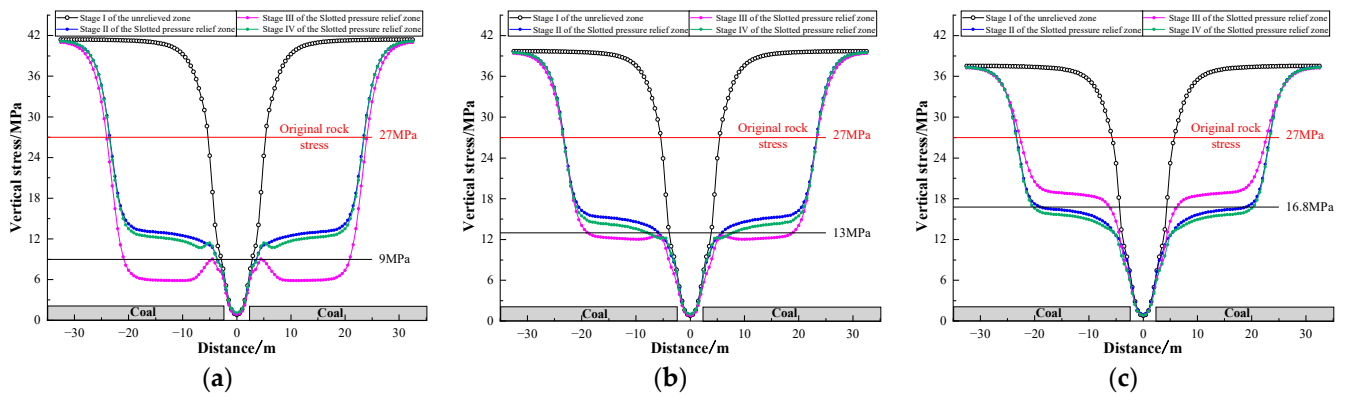


Figure 9. The vertical stress curve of the coal rib zone in the roadway with the borehole spacing of 4.0 m (a), 5.0 m (b), and 6.0 m (c).

(3) Variation rule of plastic zone

The variation rule of the plastic zone is shown in Figure 10a, in which the coal rib zone around the slot is a shear failure. The widths of the failure are about 1.5 m and 0.5 m in the X and Z directions, respectively. When the plastic zone around the roadway is evaluated, both tensile and shear failure coexist and the distance to the roadway wall, floor, and roof are 0.6 m, 0.4 m, and 1.2 m, respectively. In general, the plastic zone of the pressure-releasing area decreases gradually with the increased distance between drilling holes.

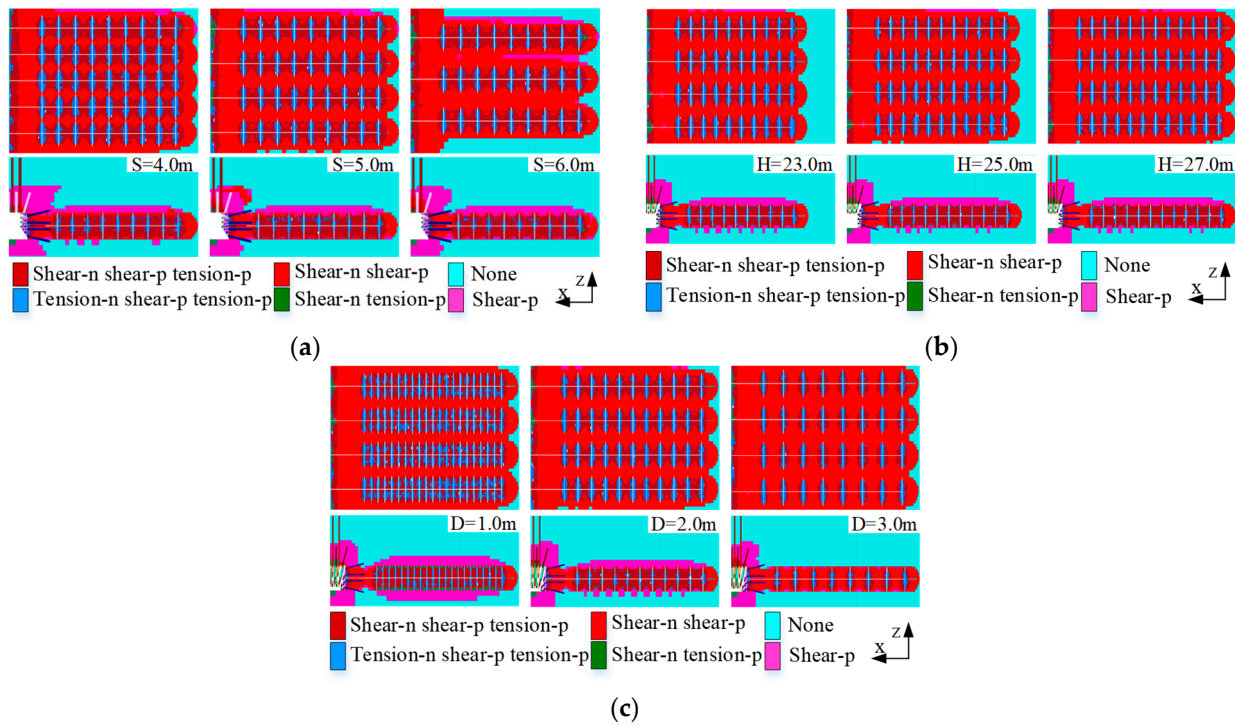


Figure 10. The change law of the plastic zone under different parameters: drilling spacing and slit radius (a), drilling depth and slit length (b), and slot cutting spacing and slot cutting width (c).

(4) Change the rule of elastic energy

It is shown in Figure 11a that these energy-gathering areas in the roof and floor area of the roadway without seam relief are either the “oval” or the “annular”. The elastic energy decreases significantly in the area of 5.0 m in the lane wall and around the seam. When the spaces between holes were 4.0 m, 5.0 m, and 6.0 m, the average elastic energy density in the pressure relief zone decreased to 0.048 MJ, 0.063 MJ, and 0.084 MJ, respectively. Compared

with the average flexible energy density before the application of the pressure relief, the reduction rates were 63.6%, 52.3%, and 36.4%, respectively.

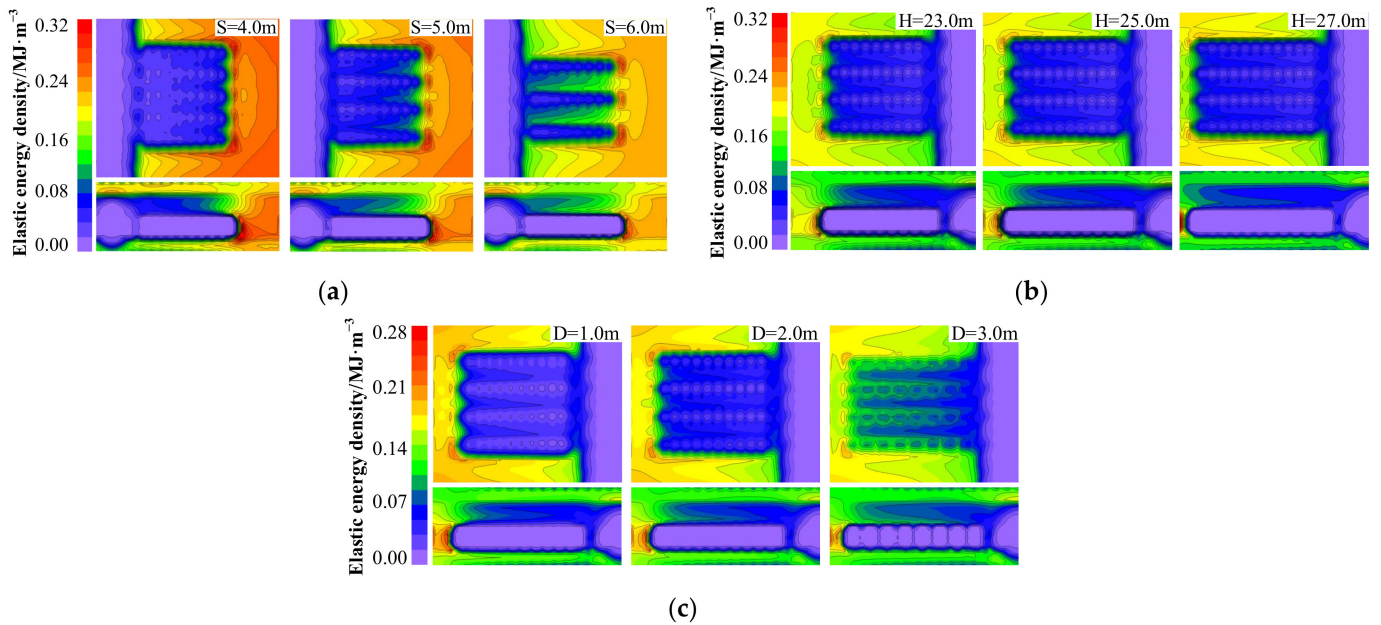


Figure 11. Diagram of the change law of elastic energy density under different parameters: drilling spacing and slit radius (a), drilling depth and slit length (b), and slot cutting spacing and slot cutting width (c). Evaluation of roadway impact risk index.

The compressive strength of No.3 coal (σ_c) is 21.1 MPa with the elastic modulus (E) of 3490 MPa. As a result, the value of U_{min} is 0.0638 MJ. Note that the shock hazard index K values are shown in Figure 12a. When the borehole spacings are 4.0 m, 5.0 m, and 6.0 m, the values of the unloading zone average impact risk index K are 0.75, 0.98, and 1.32.

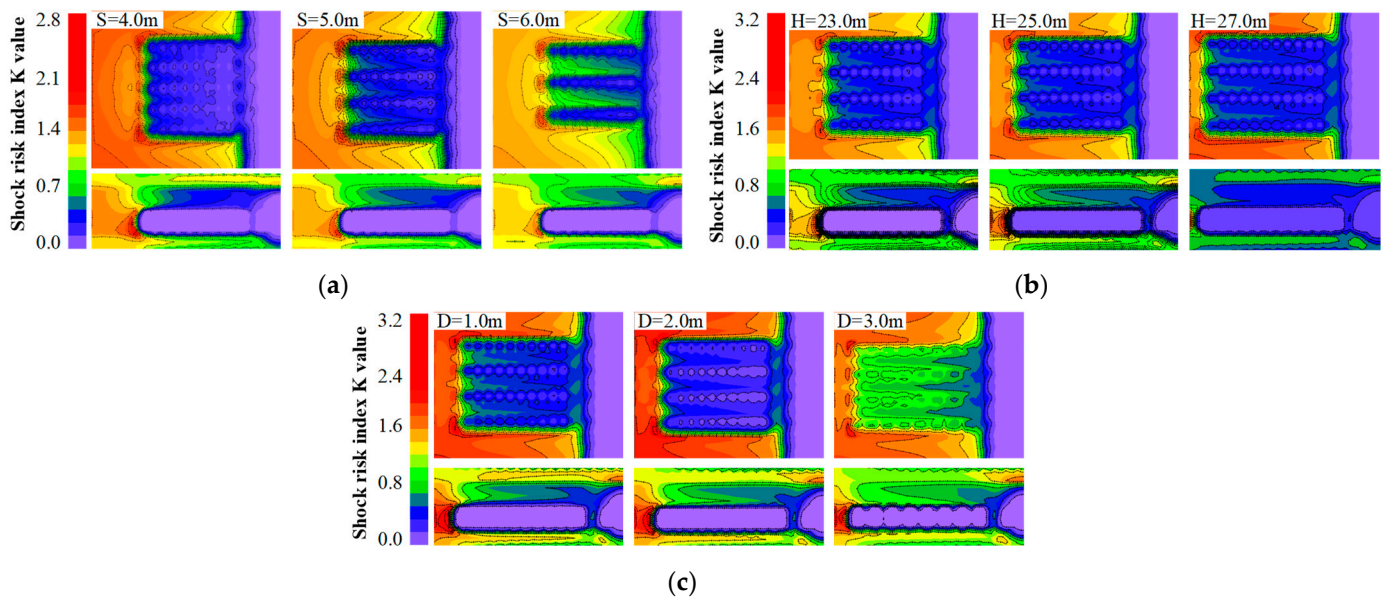


Figure 12. Variation chart of K value of shock risk index under different parameters: drilling spacing and slit radius (a), drilling depth and slit length (b), and slot cutting spacing and slot cutting width (c).

(5) Optimum parameters

It can be concluded that the parameters of the hole spacing and the slit radius of the HPWJ slotting have a significant influence on the effect of the pressure releasing. In general,

the larger the slit radius is, the higher the pressure relief effect is. Moreover, the larger the hole spacing is, the lower the pressure relief effect is. Among them, the Project 10, 18, and 19, that is, the spacing between the holes and the radius of the slit is 3.0 m–1.5 m, 4.0 m–2.0 m, and 5.0 m–2.0 m, respectively, have a better pressure-releasing effect. The pressure-releasing effect data of the above three schemes are listed in Table 5. When these four parameters (e.g., average vertical stress of coal rib zone, elastic energy density, impact risk index K value, and pressure relief cost estimation) were comprehensively considered, the pressure-releasing effect of the Project 19 was the best, when the spacing between the boreholes and slit radius was 5.0 m–2.0 m, respectively.

Table 5. Data table of pressure relief effect under the condition of drilling distance–cut gap radius parameter.

The Project	The Borehole Spacing/m	The Slot Radius/m	Average Vertical Stress/MPa	Average Elastic Energy Density/MJ	Roadway Impact Risk Index		Pressure Relief Cost Estimation
					Central Roadway	Top, Bottom	
10	3.0	1.5	11	0.053	0.82	2.25	70 cutting slots
18	4.0	2.0	9	0.048	0.75	2.2	50 cutting slots
19	5.0	2.0	13	0.063	0.98	2.2	40 cutting slots

3.3.2. Analysis of Drilling Depth and Slit Length Parameters

Taking the borehole depth–slit length of 23.0 m–18.0 m, 25.0 m–20.0 m, and 27.0 m–22.0 m as examples, the variation rules of parameters (e.g., the movement field, stress field, plastic zone, and elastic energy density of the roadway side after pressure relief) were analyzed in this section.

(1) Changing the rule of the displacement field

The variation rule of the displacement field is shown in Figure 7b. Attributed to the existence of the roadway wall support, the wall displacement is small in general. When the borehole depth is 27.0 m, the maximum value is only 3.14 mm.

(2) Variation law of stress field

It is shown in Figure 13 that the vertical stress in the unloading area of the roadway decreases to the original rock stress, with average vertical stress of 15 MPa. In this situation, the stress concentration coefficient is 0.56 and the stress concentration only occurred 6.0m apart from the roadway wall, with average vertical stress of 16.5 MPa and a concentration coefficient of 0.61.

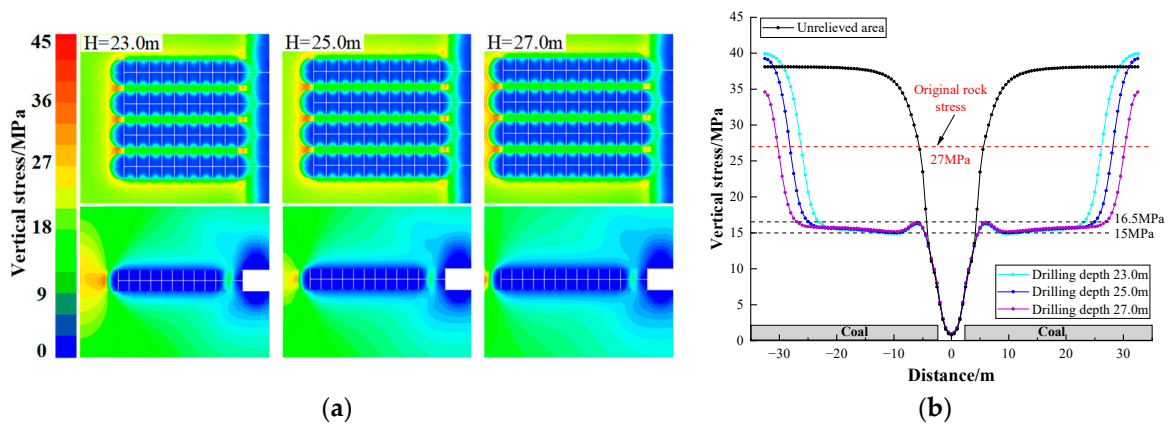


Figure 13. Stress field change cloud map (a); stress field change curve (b).

Within the range of 0–3 m at the bottom of the drill hole, the phenomenon of stress concentration was attributed to the disturbance of groove cutting. The centerline of the drill hole was symmetrically distributed into being “fan-shaped” and the average peak

value of vertical stress was about 37.7 MPa with a stress concentration coefficient of 1.40. Generally speaking, the peak value of vertical stress is more significant with the increased depth of the borehole.

(3) Variation rule of plastic zone

It is interesting in Figure 10b that the coal rib zone around the slit hole is featured with a shear failure, whereby the width of which is about 1.5 m along the X direction and 0.3 m along the Z direction. When the plastic zone around the roadway was investigated, the tensile failure and shear failure coexisted in the range of the roadway wall at about 0.6 m, the floor at about 0.4 m, and the roof at about 1.2 m. As the drilling depth increased, the plastic zone of the pressure relief area increased gradually.

(4) Variation rule of elastic energy density

It is shown in Figure 11b that the elastic energy in the coal rib zone decreased to a certain extent and the decreased elastic energy in the roadway wall exhibited a gradual decrease after pressure relief at the HPWJ cutting seam. When the drilling depths were 23.0 m, 25.0 m, and 27.0 m, the average flexible energy density in the pressure relief zone decreased to 0.069 MJ, 0.070 MJ, and 0.072 MJ, respectively. Compared with the average elastic energy density before pressure relief of 0.132 MJ, the reduction rates were 47.7%, 47.0%, and 45.5%, respectively.

(5) Evaluation of roadway impact risk index

As per Figure 12b, the average values of the impact risk index in the pressure relief zone were 1.08, 1.10, and 1.12, respectively, when the drilling depths were 23.0 m, 25.0 m, and 27.0 m. Moreover, the average value of the K around the roof and floor of the roadway was about 2.2, whereas the values of the impact risk index of the coal area around the bottom of the borehole were within the range of 2.8–3.0.

(6) Optimum parameters

Theoretically speaking, the HPWJ cutting technique parameters on the drilling depth-slotted length of high and low impact were more significant. In general, the greater the pressure-releasing belt formed, the more significant the higher pressure-releasing effect. However, the drilling depth is not infinite, in fact. When H is equal to 25 m, the lane of 20 m within the scope of the vertical stress will decrease to the original rock stress with the stress concentration coefficient of 0.56. When the lengths of the unslit are 3.0 m and 5.0 m, the vertical stress in the relief zone will be smaller than that of the original rock, and when the depth of the borehole is increased to 25 m, the peak value of the vertical stress is 15.5 MPa and 16.5 MPa, respectively. Considering the existence of an on-site roadway support and the maximization of the pressure relief effect to maintain the overall stability of the roadway, the length of the uncut joint is set up to 5.0 m. In this case, the optimal combination of the drilling depth and slit length is 25.0 m–20.0 m.

3.3.3. Analysis of Slot Cutting Spacing and Slot Cutting Width Parameters

Taking the slot cutting width of 0.1 m as an example, the variation rules of the displacement field, stress field, plastic zone, and the elastic energy density of the roadway side after pressure relief were analyzed when the slot cutting spacing was 1.0 m, 2.0 m, and 3.0 m.

(1) Changing rule of displacement field

The variation rule of the displacement field is shown in Figure 7c, in which the existence of the roadway wall support was considered. It is apparent that the wall displacement is small. In particular, the maximum value is 3.14 mm, when the groove cutting interval is 1.0 m.

(2) Variation law of stress field

It is shown in Figure 14 that the stress concentration exists in the area 6.0 m away from the roadway side, while the vertical stress is about 16.6 MPa. The average vertical stresses within the pressure relief zone are 10.95 MPa, 13.33 MPa, and 18.05 MPa, and when the groove cutting spaces are 1.0 m, 2.0 m, and 3.0 m, respectively, the stress concentration coefficient is 0.41, 0.49, and 0.67, respectively. When the slot cutting distance is 3.0 m, the stress is about 18.4 MPa, and the stress concentration of the coal rib zone is obvious. In general, the pressure relief effect becomes worse with the increase in the slot cutting distance.

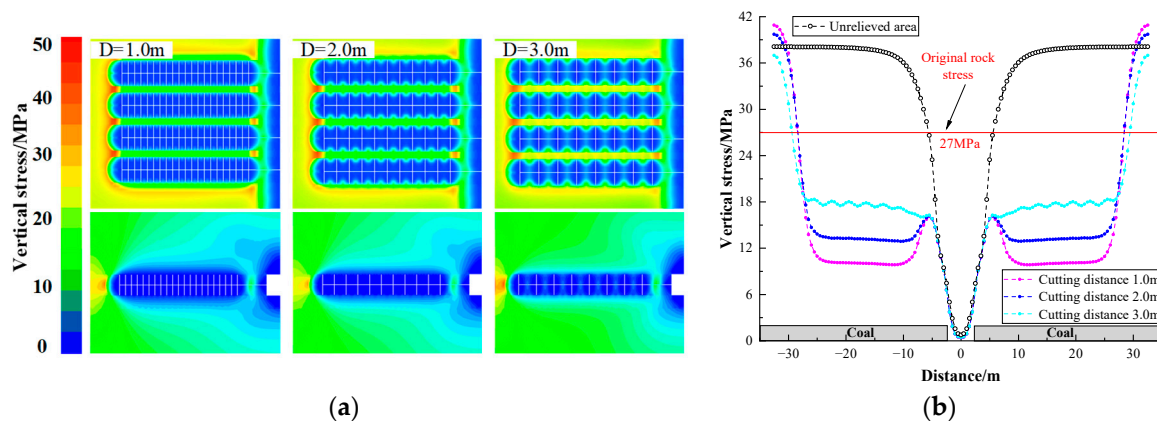


Figure 14. Stress field change cloud map (a); stress field change curve (b).

(3) Variation rule of plastic zone

When the variation rule of the plastic zone shown in Figure 10c was analyzed, the coal rib zone around the slit hole was featured with the shear failure, whereby the widths of which were about 1.5 m and 0.5 m in the X and Z directions. For the coal plastic zone around the roadway, tensile failure and shear failure coexisted within the range of the roadway wall (0.6 m) and the floor (0.4 m), as well as the roof (1.2 m). That is, the content of the plastic zone decreased with the increased slot spacing.

(4) Variation rule of elastic energy density

It is shown in Figure 11c that the elastic energy in the coal rib zone decreases after the pressure release at the HPWJ cutting seam. Meanwhile, the accumulated elastic energy in the roadway wall exhibited a gradual decrement. The average flexible energy density within the pressure relief zone with slot spacing of 1.0 m, 2.0 m, and 3.0 m decreased to 0.054 MJ, 0.069 MJ, and 0.098 MJ, respectively. Compared with the average elastic energy density before the pressure relief (0.132 MJ), the reduction rates were 59.1%, 47.7%, and 25.8%, respectively.

(5) Evaluation of roadway impact risk index

The average values of the impact risk index (K) value in the unloading area, as depicted in Figure 12c, are 0.86, 0.98, and 1.5, when the slot cutting interval is 1.0 m, 2.0 m, and 3.0 m. In addition, the average value of the impact risk index K value in the coal area around the roadway roof and floor is about 2.35, whereas the K value of the coal impact risk index at the bottom of the borehole is about 2.8–3.2.

(6) Optimum parameters

To sum up, the groove cutting spacing–groove cutting width of the HPWJ cutting are the critical parameters affecting the feasibility of the pressure relief. The larger the groove cutting spacing is, the higher the stress concentration between the grooves is, and vice versa. Among them, Schemes 1, 2, 3, 4, 5, and 6, namely slot cutting spacing–slot cutting width of 1.0 m–0.1 m, 1.0 m–0.2 m, 1.0 m–0.3 m, 2.0 m–0.1 m, 2.0 m–0.2 m, and 2.0 m–0.3 m, exhibited a better pressure relief effect. As shown in Table 6, the elastic energy density, the impact of the risk index K value, and the unloading cost estimates for the total length

(single-slot cutting–drilling) were comprehensively evaluated. That is, Plan 1 with the slot cutting spacing–slot cutting width of 1.0 m–0.1 m unloading obtained the best effect.

Table 6. Data table of pressure relief effect under the condition of slot cutting distance–slot cutting width parameter.

The Project	Cutting Spacing/m	Cutting Width/m	Average Vertical Stress/MPa	Average Elastic Energy Density/MJ	Roadway Impact Risk Index			Pressure Relief Cost (Number of Slots × Width of Slots)
					Central Roadway	Top, Bottom	The Bottom of the Hole	
1	1.0	0.1	10.95	0.054	0.86	2.4	3.2	21 × 0.1 = 2.1 m
2	1.0	0.2	10.86	0.053	0.83	2.4	3.2	17 × 0.2 = 3.4 m
3	1.0	0.3	10.63	0.053	0.82	2.3	3.4	16 × 0.3 = 4.8 m
4	2.0	0.1	13.33	0.069	0.98	2.4	3.2	11 × 0.1 = 1.1 m
5	2.0	0.2	13.20	0.069	0.98	2.4	3.2	10 × 0.2 = 2.0 m
6	2.0	0.3	13.16	0.067	0.97	2.3	3.2	10 × 0.3 = 3.0 m

4. Engineering Case Study

4.1. Engineering Background

The central coal rib zone in the 730 mining area of a mine had substantial bursting liability, and the roof and floor had weak bursting liability. The thickness of the coal seam is 8.9~10.6 m, with an average thickness of 10.2 m. The buried depth of the coal seam is 930 m~1300 m, with an average value of 1115 m. The centralized roadway in the 730 mining area is driven along the coal seam floor and the spacing between the two centralized lanes is 60 m. As depicted in Figure 15, the roadway is connected by three connecting lanes and the average buried depth of the roadway is about 1082 m. The working face is closed to the mining area concentrated lane and the concentrated lane faces abutment pressure on both sides of the superposition area. After relief engineering, such as bottom breaking construction, bottom coal replacement, and large-diameter pressure relief, CT inversion analysis was carried out on the 730 central lane area, and in the areas of A, B, and C, three high apparent wave velocity anomalies formed.

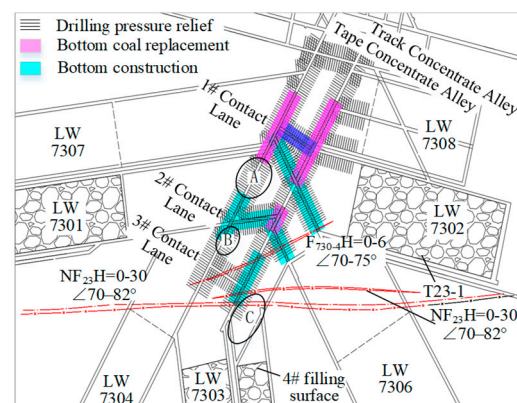


Figure 15. Layout of centralized roadway in 730 mining area.

4.2. Analysis of Influencing Factors of Rock Burst

At present, the stress centralization appears in many areas of the concentrated roadway within the 730 mining area by working faces on both sides. Some parameters including the coal rock bursting liability, deadweight stress field, mining activities, roof, geological structure, and other factors are listed below for further analysis:

- (1) The centralized roadway in the 730 mining area is located on the floor of the No. 3 coal seam. This coal seam is of substantial bursting liability with an average compressive strength of 22.7 MPa. The direct roof and low rock strata are mudstones, and the average compressive strength is 28.6 MPa. The small strength stress ratio leads to the quick failure of the roadway after excavation.
- (2) The larger buried depth of the concentrated roadway results in the higher deadweight stress applied on the roadway roof, which exceeds the UCS of the coal seam. In

this case, the elastic energy accumulated in the coal seam increases greatly with the mining depth.

- (3) The adjacent working faces (e.g., 7301, 7302, 7303, and 7305) were all extracted and these protective coal pillars of the main roadway in front of the stop-mining line are not only subjected to the gravity load of the roof strata but are also subjected to the joint action of the part of the rock loads. This is believed to be the main reason for the high-stress concentration after being superimposed in the concentrated roadway area.
- (4) The folds of the concentrated roadway in the 730 mining area are relatively developed. F730-4, F730-5, and NF23 faults are exposed and the fault drop is significant. Affected by the mining stress field of the working face on both sides, the fault area has a high risk of roadway instability failure.

Combined with the actual situation of the concentrated roadway and the impact factors mentioned above, it can be concluded that the high deadweight stress field, the abutment pressure attributed to the mining activities of the working faces on both sides, and the high-stress action caused by the tectonic stress field formed by faults and folds, are the leading static load sources in the concentrated roadway area.

4.3. Pressure Relief Scheme Design

The HPWJ cutting and pressure relief measures were applied in No.3 connecting the roadway side in the 730 mining area. Six pairs of the HPWJ cutting and drilling holes were implemented. As shown in Figure 16, the stress-relaxation area of the roadway side coal seam is 25 m. The HPWJ slotting technology hole spacing $S = 5.0$ m, the slotting radius $RC = 2.0$ m, the hole depth $H = 25$ m, the slit length $L = 20.0$ m, the slot cutting spacing = 1.0 m, the slot cutting width = 0.1 m, and the drilling location is 1.5 m above the roadway floor. The ZGF-100(A)-type HPWJ cutting device was adopted to drill the borehole with a diameter of 113 mm.

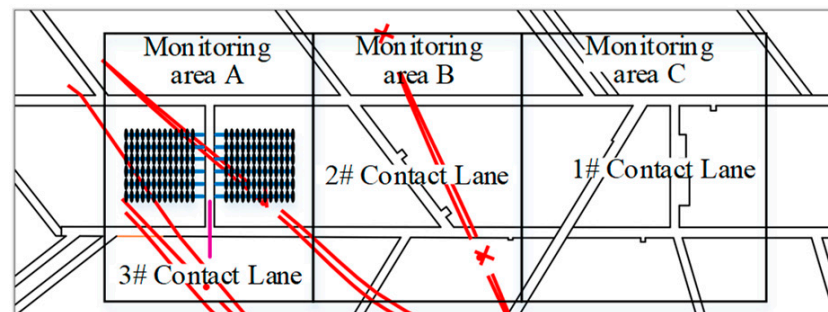


Figure 16. Layout of water jet slotting pressure relief.

4.4. Pressure Relief Effect Inspection

Statistics were made on the microseismic eventssituation of No.3 contact lanes in the 730 mining area before and after the application of the HPWJ cutting and pressure releasing. Detailed information about the key results can be seen in Table 7.

Considering that there is no energy event with the energy larger than 10^4 J, microseismic events with energy $E > 10^3$ J and $E \leq 10^3$ J are defined as high-energy-level and low-energy-level events, respectively. It was on 20 June 2020 that the HPWJ slit pressure relief was carried out on both sides of the No.3 connecting roadways. Within one week before pressure relief, 28 microseismic events occurred in the area near the centralized roadway with a total energy of 2.49×10^4 J and a daily microseismic frequency of 4/d. That is, the occurrence frequency of high-energy microseismic events was limited, and only accounted for 25.0%.

Table 7. Statistical table of microseism events before and after pressure relief of No. 3 connecting roadway.

Date	State of Roadway	Seismic Frequency	The Total Energy/J	Daily Frequency/(d)	Microseismic Level Statistics			Microseismic Concentration Statistics			
					The Energy Levels	Frequency	Proportion	Area	Frequency	Proportion	Concentration (/m)
14 June 2020 – 20 June 2020	Before pressure relief	28	2.49×10^4	4	High energy level	7	25.0%	A	2	28.6%	0.007
								B	3	42.8%	0.010
								C	2	28.6%	0.007
					Low level	21	75.0%	A	8	38.1%	0.027
								B	6	28.6%	0.020
								C	7	33.3%	0.023
21 June 2020 – 27 June 2020	After pressure relief	19	1.52×10^4	2.71	High energy level	3	15.79%	A	0	0	0
								B	2	66.7%	0.006
								C	1	33.3%	0.003
					Low level	16	84.21%	A	5	31.3%	0.015
								B	5	31.3%	0.015
								C	6	37.4%	0.018
28 June 2020 – 4 July 2020	After pressure relief	13	9.88×10^3	1.86	High energy level	3	23.08%	A	2	66.7%	0.006
								B	0	0	0
								C	1	33.3%	0.003
					Low level	10	76.92%	A	3	30.0%	0.009
								B	2	20.0%	0.006
								C	5	50.0%	0.015

After the pressure relief via the high-pressure water jet cutting, 19 microseismic events were monitored in the first week and 13 microseismic events occurred during the second week. The microseismic frequency decreased significantly and the total energy was 1.52×10^4 J and 9.88×10^4 J, which fell by 38.96% and 60.32%. The daily frequencies of microearthquakes were 2.71/d and 1.86/d, respectively, which decreased by 32.25% and 53.50% compared with those before pressure relief. The proportion of high-level microseismic events decreased significantly: 15.79% and 23.08%.

Statistical analysis was conducted on the spatial concentration of high- and low-level microseismic events in different areas of the centralized roadway before and after pressure relief. By comparing the spatial concentration of high- and low-level microseismic events in the A, B, and C areas in the No. 3 contact lane, as shown in Table 7, the spatial concentration of high-level microseismic events in the B area was the highest at 0.01 during 06.14–06.20 before pressure relief, whereas the spatial concentration of high-level microseismic events in the B area decreased by 40% during 06.21–06.27 after pressure relief. Before the pressure relief, the microseismic spatial concentration of a low energy level in 06.14–06.20 was the highest in region A: 0.027. After the pressure relief, the microseismic spatial concentration in region A decreased by 44.4% and 66.7% in 06.21–06.27 and 06.28–07.04. Compared with that in area C, the spatial concentration of the high-energy-level microseismic events in 06.21–06.27 and 06.28–07.04 after pressure relief decreased by 57.1%. The spatial aggregation degree of the low-energy-level microseismic events in region C was 21.7% and 34.8% lower than that before the pressure relief, respectively. Therefore, it can be seen that the No.3 contact lane adopts the HPWJ cutting scheme designed in the present research. In particular, the pressure relief effect is evident in areas A, B, and C, suggesting that it is effective in achieving the safety production of the working face.

5. Discussions

For a certain rock burst risk area, the pressure relief effect of the HPWJ constructed according to the designed pressure relief parameters will also be affected by the environmental factors of the coal seam, of which the strength of the coal body has the greatest impact. In Sections 2 and 3, the influence of the design parameters of pressure relief on the effect of pressure relief was studied according to the specific strength of the coal seam, but the influence of the strength of the coal mass on the effect of pressure relief was not considered.

In this paper, the optimal pressure relief parameters derived above for high-pressure water jets were used to conduct numerical simulation research on six types of coal with different uniaxial compressive strengths of 10.0, 15.0, 20.0, 25.0, 30.0, and 35.0 MPa, respectively, to analyze the impact of coal strength on the pressure relief effect. The two main indicators selected were vertical stress and impact risk index for the study.

As illustrated in Figure 17, in the pressure relief area, when the compressive strength of the coal varies from 10.0 MPa to 35.0 MPa, the vertical stress changes slightly, with a

gentle distribution, and there is no obvious stress concentration area. The average vertical stress in the slit area is about 13.7 MPa, 14.9 MPa, 15.8 MPa, 16.8 MPa, 17.7 MPa, and 18.5 MPa, respectively, and the stress concentration coefficients are 0.51, 0.55, 0.59, 0.62, 0.66, and 0.69. There is a phenomenon of stress concentration in the area around 6.0m from the roadway wall, with peak values of 18.46 MPa, 19.08 MPa, 20.69 MPa, 21.92 MPa, and 23.75 MPa, respectively. The change area of the peak value is positively correlated with the compressive strength of the coal. Although there is a peak value, the vertical stress in the pressure relief area is lower than the original rock stress (27 MPa). However, within the range of 0~3 m from the bottom of the borehole due to the disturbance of the slot, there is a phenomenon of stress concentration, which is symmetrically distributed in a “fan shaped” shape along the centerline of the borehole. The average vertical stress peak can reach about 49 MPa, and the stress concentration coefficient is 1.81. As the compressive strength of the coal body increases, the greater the disturbance within the range of 0~3 m from the bottom of the borehole becomes.

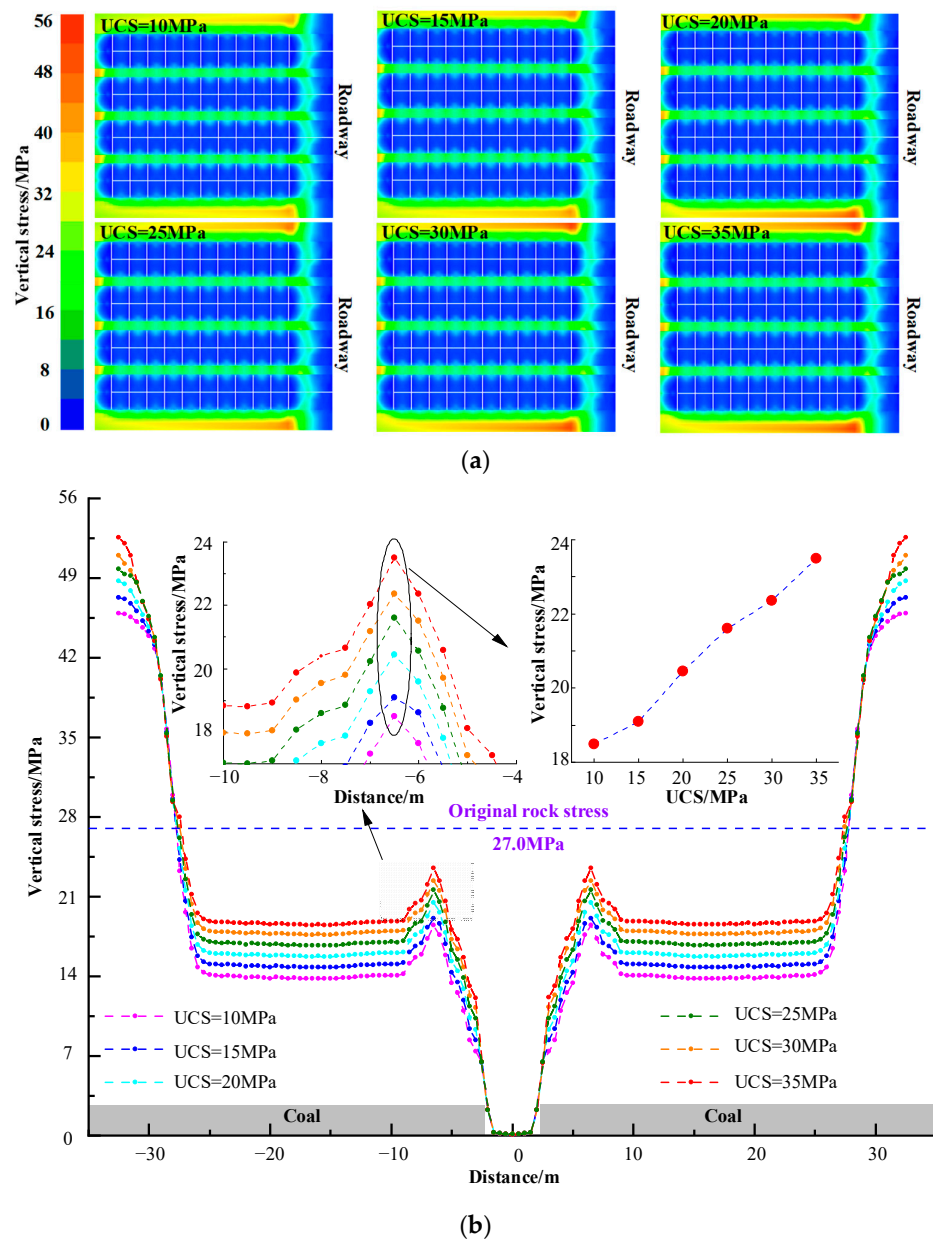


Figure 17. Change law of stress field of roadway surrounding coal with different strengths: stress cloud (a) and stress curves (b).

Figure 18 depicted a variation chart of the K value of the shock risk index under different coal strengths (10.0–35.0 MPa). After pressure relief using the HPWJ, the elastic energy accumulated in the coal seam decreased to some extent, and the average elastic energy density in the pressure relief zone of the compressive strength of each coal body decreased to 0.058 MJ, 0.06 MJ, 0.07 MJ, 0.08 MJ, 0.09 MJ, and 0.115 MJ, respectively. The corresponding average K values of the shock risk index were 0.34, 0.46, 0.67, 1.03, 1.28, and 1.62, respectively. Only when the compressive strength of the coal body was 10.0, 15.0, and 20.0 MPa, the K value was less than 1, with a certain pressure relief effect. As the compressive strength of coal increases, the average value of the K in the pressure relief zone is still greater than 1, indicating a certain impact risk.

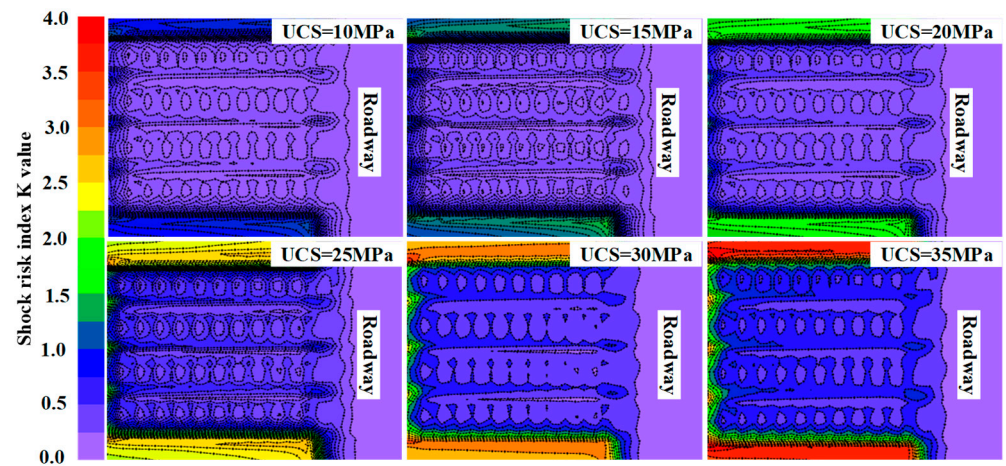


Figure 18. Variation chart of K value of shock risk index under different coal strengths.

According to the above analysis results, the strength of the coal seam has a significant impact on the pressure relief effect of the HPWJ. As the compressive strength of the coal seam increases, the stress of the coal mass within the pressure relief range increases, but they are both below the original rock stress. The elastic energy density and impact risk index K value both increase with the increase in the compressive strength of the coal seam. In general, the pressure relief effect of HPWJ is greatly affected by the compressive strength of the coal seam, which is inversely proportional.

6. Conclusions

- (1) Based on the analysis of the pressure relief principle of the HPWJ, combined with the actual needs of on-site application of the technology, theoretical analysis was conducted for six key pressure relief design parameters on site. Theoretical calculation models were established for drilling spacing–slit radius, drilling depth–slit length, and slotting cutting spacing–slotting cutting width, respectively. Based on the specific physical and mechanical properties of coal seams, reasonable theoretical interval values for pressure relief parameter design can be obtained;
- (2) According to the theoretical interval values of pressure relief parameters, the theoretical values of pressure relief parameters were simulated and analyzed using numerical simulation. Based on the research and judgment of the displacement, vertical stress, plastic zone, elastic energy, and impact risk index, combined with the field pressure relief cost, the optimal pressure relief parameters were obtained;
- (3) For the rock burst risk area in the case, the optimal design parameters determined via theoretical analysis and numerical simulation were used to carry out the relief work of HPWJ on both sides of the No.3 connecting the roadway. By comparing the microseismic frequency, total energy, and spatial concentration of high and low energy levels before and after pressure relief, there was a significant decrease in all indicators after pressure relief, and the effect of pressure relief was obvious, which played a greater role in reducing the risk of impact ground pressure coal seams.

Author Contributions: Conceptualization, Y.W. and A.C.; methodology, Y.W. and A.C.; software, Y.W., C.D. and Y.H.; validation, S.S.; formal analysis, C.X. and Y.P.; investigation, Y.W.; resources, A.C.; data curation, Y.W.; writing—original draft preparation, Y.W. and A.C.; writing—review and editing, A.C.; supervision, Y.W. and A.C.; project administration, Y.W. and S.S.; funding acquisition, A.C. All authors have read and agreed to the published version of the manuscript.

Funding: This research was funded by the National Natural Science Foundation of China (No. 52274098 and U21A20110), and National Key Research and Development Program of China (2022YFC3004603).

Institutional Review Board Statement: Not applicable.

Informed Consent Statement: Not applicable.

Data Availability Statement: All data generated or analyzed during this study have been included in this article.

Acknowledgments: The authors are grateful to Shaanxi Zhengtong Coal Ind Co Ltd. for providing field testing. The authors would also like to thank the peer reviewers and editors for their valuable comments and suggestions, which have greatly improved the manuscript presentation.

Conflicts of Interest: The authors declare no conflict of interest.

References

1. Dou, L.M.; Chen, T.J.; Gong, S.Y.; He, H.; Zhang, S.B. Rockburst hazard determination by using computed tomography technology in deep workface. *Saf. Sci.* **2012**, *50*, 736–740. [[CrossRef](#)]
2. Vazaios, I.; Diederichs, M.S.; Vlachopoulos, N. Assessment of strain bursting in deep tunnelling by using the finite-discrete element method. *J. Rock Mech. Geotech. Eng.* **2019**, *11*, 12–37. [[CrossRef](#)]
3. Yang, S.; Lian, H.; Xu, B.; Thanh, H.V.; Chen, W.; Yin, H.; Dai, Z. Application of robust deep learning models to predict mine water inflow: Implication for groundwater environment management. *Sci. Total Environ.* **2023**, *871*, 162056. [[CrossRef](#)] [[PubMed](#)]
4. Zhang, Z.; Ning, J.G.; Wang, J.; Wang, K.; Yang, S.; Yan, R.Y.; Sun, G.Q.; Du, M.H. Coal Pillar Stress Weakening Technology and Application by Gob-Side Entry Driving and Hydraulic Roof Cutting in Deep Shafts Mines. *Processes* **2022**, *10*, 827. [[CrossRef](#)]
5. Zhao, H.C.; Ren, T.; Remennikov, A. A hybrid tubular standing support for underground mines: Compressive behaviour. *Int. J. Min. Sci. Technol.* **2021**, *31*, 215–224. [[CrossRef](#)]
6. Xue, C.C.; Cao, A.Y.; Guo, W.H.; Liu, Y.Q.; Wang, S.W.; Dong, J.Y.; Gu, Y. Mechanism and Energy Evolution Characteristics of Coal Burst in Mining Thick, Deep, and Large Inclined Coal Seams: A Case Study from a Chinese Coal Mine. *Geofluids* **2022**, *2022*, 7704226. [[CrossRef](#)]
7. Cao, A.Y.; Liu, Y.Q.; Jiang, S.Q.; Hao, Q.; Peng, Y.J.; Bai, X.X.; Yang, X. Numerical Investigation on Influence of Two Combined Faults and Its Structure Features on Rock Burst Mechanism. *Minerals* **2021**, *11*, 1438. [[CrossRef](#)]
8. Dai, L.P.; Pan, Y.S.; Li, Z.H.; Wang, A.W.; Xiao, Y.H.; Liu, F.Y.; Shi, T.W.; Zheng, W.H. Quantitative mechanism of roadway rockbursts in deep extra-thick coal seams: Theory and case histories. *Tunn. Undergr. Space Technol.* **2021**, *111*, 103861. [[CrossRef](#)]
9. Shen, C.M.; Lin, B.Q.; Sun, C.; Zhang, Q.Z.; Li, Q.Z. Analysis of the stress-permeability coupling property in water jet slotting coal and its impact on methane drainage. *J. Pet. Sci. Eng.* **2015**, *126*, 231–241. [[CrossRef](#)]
10. Zhang, J.G.; Zhang, J.J.; Zhou, Z. Investigation of a Self-Excited Pulsed Water Jet Slotting for Coal Roadway Driving. In Proceedings of the 2nd International Conference on Advances in Mechanical Engineering and Industrial Informatics (AMEII), Hangzhou, China, 9–10 April 2016; pp. 475–481.
11. Yang, Z.Q.; Liu, C.; Jin, H.W. Study on Pressure Relief Zone Formed Inside Roadway Rib by Rotary Cutting with Pressurized Water Jet for Preventing Rock Burst. *Adv. Civ. Eng.* **2022**, *2022*, 9647029. [[CrossRef](#)]
12. Cheng, X.Y.; Zhang, Q.H.; Zhang, Z.G.; Zou, Y.L.; Guo, J.J. Stress Relief and Stimulation of Coal Reservoir by Hydraulic Slotting. *Adv. Civ. Eng.* **2021**, *2021*, 6664696. [[CrossRef](#)]
13. Zhang, J.L.; Yang, F.W.; Cao, Z.G.; Xia, Y.M.; Li, Y.C. In situ experimental study on TBM excavation with high-pressure water-jet-assisted rock breaking. *J. Cent. South Univ.* **2022**, *29*, 4066–4077. [[CrossRef](#)]
14. Chen, L.H.; Cheng, M.Z.; Cai, Y.; Guo, L.W.; Gao, D.R. Multi-Objective Collaborative Optimization Design of Key Structural Parameters for Coal Breaking and Punching Nozzle. *Processes* **2022**, *10*, 1036. [[CrossRef](#)]
15. Cao, S.R.; Ge, Z.L.; Zhang, D.; Zhou, Z.; Lu, Y.Y.; Zhao, H.Y. An experimental study of ultra-high pressure water jet-induced fracture mechanisms and pore size evolution in reservoir rocks. *Int. J. Rock Mech. Min. Sci.* **2022**, *150*, 14. [[CrossRef](#)]
16. Xue, Y.Z.; Si, H.; Chen, G.H. The fragmentation mechanism of coal impacted by water jets and abrasive jets. *Powder Technol.* **2020**, *361*, 849–859. [[CrossRef](#)]
17. Zhang, Y.J. Study on the Theory of High Pressure Water Jet Coal Breaking and Its Main Controlling Factors. In Proceedings of the 7th Annual International Conference on Material Science and Environmental Engineering (MSEE), Wuhan, China, 15–16 November 2019.

18. Lu, Y.Y.; Liu, Y.; Li, X.H.; Kang, Y. A new method of drilling long boreholes in low permeability coal by improving its permeability. *Int. J. Coal Geol.* **2010**, *84*, 94–102. [[CrossRef](#)]
19. Deepak, D.; Jodel, A.Q.C.; Abraham, M.M.; Prasad, U.S. Technology. Numerical Analysis of The Effect of Nozzle Geometry on Flow Parameters in Abrasive Water Jet Machines. *Pertanika J. Sci. Technol.* **2017**, *25*, 497.
20. Jiang, T.W.; Huang, Z.W.; Li, J.B.; Li, H. Effect of parameters on threshold pressure of sandstone tested by water jet. *Int. J. Rock Mech. Min. Sci.* **2021**, *139*, 104640. [[CrossRef](#)]
21. Nair, A.; Khan, M.A.; Sivakumar, M.; Selvaganesh, R.M.; Sushanth, J.; Sachin, M. Geometric characteristics analysis of hole making through abrasive water jet drilling. In Proceedings of the 3rd International Conference on Advanced Materials and Modern Manufacturing (ICAMMM), Chennai, India, 3–4 April 2020; pp. 338–347.
22. Zhong, J.Y.; Ge, Z.L.; Lu, Y.Y.; Zhou, Z.; Zheng, J.W. New Mechanical Model of Slotting-Directional Hydraulic Fracturing and Experimental Study for Coalbed Methane Development. *Nat. Resour. Res.* **2021**, *30*, 639–656. [[CrossRef](#)]
23. Gu, B.F.; Deng, Y.L.; Shi, Y. Simulation Study of Coal Failure Law under High-Pressure Water Jetting. *Teh. Vjesn.* **2020**, *27*, 1800–1806.
24. Li, C. Experimental Study Via Dynamic Prediction Model on High Pressure Hydraulic Slotting and High Efficiency Gas Drainage Technology under Complex Geological Conditions. *J. Phys. Conf. Ser.* **2021**, *1769*, 012021–012028. [[CrossRef](#)]
25. Gao, F.; Xue, Y.; Gao, Y.A.; Zhang, Z.Z.; Teng, T.; Liang, X. Fully coupled thermo-hydro-mechanical model for extraction of coal seam gas with slotted boreholes. *J. Nat. Gas Sci. Eng.* **2016**, *31*, 226–235. [[CrossRef](#)]
26. Zhang, X.Z.; Wisniewski, P.; Dykas, S.; Zhang, G.J. Permeability Enhancement Properties of High-Pressure Abrasive Water Jet Flushing and Its Application in a Soft Coal Seam. *Front. Energy Res.* **2021**, *9*, 12. [[CrossRef](#)]
27. Kan, J.L.; Dou, L.M.; Li, X.W.; Li, J.Z.; Chai, Y.J. Investigating the destressing mechanism of roof deep-hole blasting for mitigating rock bursts in underground coal mines. *Geomat. Nat. Hazards Risk* **2022**, *13*, 2508–2534. [[CrossRef](#)]
28. Li, Y. New research on the stress field of elastic-plastic small deformation problems. *J. Mater. Process. Technol.* **2003**, *138*, 508–512. [[CrossRef](#)]
29. Li, Y.P.; Zhang, H.W.; Zhu, Z.J.; Guo, C. Study on safety parameters of pressure relief borehole in impact dangerous Coal seam. *Chin. J. Saf. Sci.* **2018**, *28*, 122–128.
30. Li, Y.; Yuan, L.; Liu, G.X.L.; Xue, J.H.; Yu, G.F.; Peng, Y.; Zhang, M.; Zhou, W. Determination of surrounding rock disturbance zone and critical failure depth of circular roadway. *Chin. J. Min. Saf. Eng.* **2016**, *33*, 795–799.
31. Qian, M.G.; Xu, J.L.; Wang, J.C.; Wu, Y.P. *Mine Pressure and Rock Formation Control*, 3rd ed.; China University of Mining and Technology Press: Xuzhou, China, 2021; pp. 222–226.
32. Zhao, Y.S.; Feng, Z.C.; Wan, Z.J. The principle of minimum energy for dynamic failure of rock mass. *Chin. J. Rock Mech. Eng.* **2003**, *22*, 1781.

Disclaimer/Publisher’s Note: The statements, opinions and data contained in all publications are solely those of the individual author(s) and contributor(s) and not of MDPI and/or the editor(s). MDPI and/or the editor(s) disclaim responsibility for any injury to people or property resulting from any ideas, methods, instructions or products referred to in the content.